Journal of Qassim University for Science
2023, *Vol 2* (Issue 2), pp. 105-118
Received: 15 September 2022
Revised: 23 October 2022
Accepted: 6 November 2022

JQUS

Synthesis, characterization and biological evaluation of an asymmetric NNO donor Schiff base and its transition metal structures

Salman F. Alotaibi *
Department of Chemistry, College of Science, Qassim University, Campus University, King Abdulaziz Road, Al-Malida, 51452 - P.O.Box: 6644, Buraydah, Qassim, Kingdom of Saudi Arabia.
Abuzar E. A. E. Albadri
Department of Chemistry, College of Science, Qassim University, Campus University, King Abdulaziz Road, Al-Malida, 51452 - P.O.Box: 6644, Buraydah, Qassim, Kingdom of Saudi Arabia.
Lotfi M. Aroua
Department of Chemistry, College of Science, Qassim University, Campus University, King Abdulaziz Road, Al-Malida, 51452 - P.O.Box: 6644, Buraydah, Qassim, Kingdom of Saudi Arabia.
Laboratory of Organic Structural Chemistry and Macromolecules, Department of Chemistry, Faculty of Sciences of Tunis, Tunis El-Manar University, El Manar I 2092, Tunis Tunisia.
Carthage University; Department of Chemistry, Faculty of Sciences of Bizerte, 7021 Jarzouna, Tunisia.
Ahmed N. Al-Hakimi
Department of Chemistry, College of Science, Qassim University, Campus University, King Abdulaziz Road, Al-Malida, 51452 - P.O.Box: 6644, Buraydah, Qassim, Kingdom of Saudi Arabia.
Department of Chemistry, Faculty of Sciences, Ibb University, Ibb, Yemen.

*Correspondence authors : Salman F. Alotaibi و salman.fahad58@yahoo.com

Abstract

A tridentate Schiff base ligand was manufactured via the concentration of 4-nitrobenzaldehyde, 2-hydroxybenzaldehyde, and p-phenylenediamine and structures were equipped and classified. Structural elucidation of the synthesized Schiff base ligand and its metal structures was determined by spectroscopic methods. The NMR spectroscopy confirmed the development of Schiff base ligand, manifesting the azomethine protons at 8.91 and 9.04 ppm in ^{1}HNMR spectrum and the azomethine carbons at 160.77, and 159.14 ppm in ^{13}CNMR spectrum. Moreover, The FT-IR spectroscopy assisted the detection of the prepared SB ligand and its metal structures. For instance, Absorption bands at 1662 cm^{-1} and 1530 cm^{-1} in the FT-IR spectrum of the SB ligand detected the formation of the azomethine groups, and these bands shifted to either lower or higher frequencies in the ranges of the structures, proving the management of Schiff base to the selected metals. Meanwhile, the UV-Vis spectroscopy has revealed the excitations of the n → π* transition of azomethine group at 325 nm, and therefore this transition has been shifted upon structuration along with the apparent d-d transitions. Molar conductivity and magnetic moment capacities were utilized to support the evidence of the development of the polymeric Schiff base structures. The Ni(II) and Cu(II) structures exhibited antibacterial and antifungal activities, whereas all the structures demonstrated considerable anticancer activities against SKOV3 and HeLa human cancer cells.

Keywords: Schiff base ligand; polymeric metal structures; antibacterial; antifungal; anticancer

1. Introduction

Schiff bases (SB) are an intensively studied class of organic composites with an imine (azomethine) group (>C=N–), discovered by German scientist Hugo Schiff [1,2]. These compounds, having carbon-nitrogen double bonds, are generally synthesized by refluxing primary amines with active carbonyl groups, either aldehydes or ketones [3–6]. Schiff bases may contain aryl or alkyl groups; however, these may contain 2-hydroxybenzaldehyde and are more stable owing to the conjugation effect [7–10].

In recent years, SB ligands comprising N and O donor sites have emphasized on chemists, chiefly due to their potent activities, especially in medicinal chemistry [11-15]. Schiff base ligands of 2-hydroxybenzaldehyde have been extensively studied as they play a significant role as antibacterial and antifungal drugs [16,17]. Moreover, these SB ligands act as chelating agents and coordinate to transition metal cations to form metal structures that exhibit various biological effects, including antimicrobial [18–20], antiviral and anti-inflammatory [21], cytotoxic [22], and hypoglycemic activities [23].

The Schiff bases of diamines like p-phenylenediamine can form two series of SB compounds, namely the symmetric ones when both amine groups are condensed with the same oxo-compound and asymmetric ones when two different oxo-compounds are condensed with the amine groups located at 1 and 4 positions of the benzene ring. The scope of our investigation besides the preparation and study of the coordination behavior of an asymmetric Schiff base, 2-[(E)-[4-[(E)-(4-nitrophenyl) methyleneamino] phenyl] iminomethyl] phenol, is to assess the antibacterial, antifungal and anticancer occurrences of the organized Schiff base and of its polymeric structures.

2. Materials and Methods:

2.1. Materials and Instrumentation

4-Nitrobenzaldehyde, 2-hydroxybenzaldehyde, and *p*-phenylenediamine, and the appropriate metal salts were bought from Sigma-Aldrich, Fluka and E. Merck, and utilized as obtained. Precise ethanol and DMSO were bought from Sigma-Aldrich for synthesizing Schiff base ligand and its metal structures without any further purification. ^{1}H and ^{13}C NMR spectroscopy of the Schiff base ligand was performed on Bruker 850 MHz and 213 MHz spectrometers, respectively, using DMSO-d_6 as the solvent. Electronic UV-Visible ranges were documented using the Shimadzu spectrophotometer (UV-1650PC, Japan). C, H and N analyses were conducted utilizing Eurovector CHN Elemental Analyzer (EA3000, Italy). Metal percentages were measured using Inductively Coupled Plasma (ICP 710-ES Varian). The magnetic measurements were measured on Sherwood Scientific's Magnetic Susceptibility Balances (MSBs). Thermal analyses were conducted using the Shimadzu TGA Simultaneous Measuring Instrument in a nitrogen atmosphere in the range of 0–500 °C with a heating rate of 10 °C/min. The used diffractometer is equipped with a monochromator.

2.2. Synthesis of the Schiff Base

The ligand, 2-[(E)-[4-[(E)-(4-nitrophenyl)methyleneamino]phenyl]iminomethyl]phenol, was prepared by the following process. To an enthused in a round flask solution of *p*-phenylenediamine (0.108 g, 1 mmol) and hot absolute ethanol (30 mL), a solution of 2-hydroxybenzaldehyde (0.118 g, 1 mmol) and 4-nitrobenzaldehyde (0.15 g, 1 mmol) in 20 mL absolute ethanol was integrated gradually. The combination was refluxed with heating for 4 h and stirred without heating overnight, following which the mixture's color was altered from brown to yellow. Finally, the precipitated yellow product was inaccessible by filtration and washed several times with hot absolute ethanol and vacuum-dried. Yield: 86.6%. "Decomposition Point: 160 °C. ^{1}H NMR (850.000 MHz, DMSO-d_6): δ (ppm): 13.08 (s, 1H, Ar-OH), 9.04 (s, 1H, HC=N), 8.91 (s, 1H, HC=N), 8.23-6.99 (m, 12H, Ar-H). ^{13}C NMR (213.77 MHz, DMSO-d_6) (δ, ppm): 163.6, 160.8, 159.1, 149.7, 149.3, 147.2, 142.0, 133.8, 133.1, 130.2, 124.6, 123.1, 123.04, 123.01, 122.9, 119.8, 119.7, 117.1. IR, ν(cm^{-1}): 3100(O-H), 1662(C=N), 1530(C=N), 1245(C-O). UV-Vis (DMSO), λ_{max} (nm): 250 ($\pi \rightarrow \pi^*$), 325 ($n \rightarrow \pi^*$). Elemental Analysis (%) For $C_{20}H_{15}N_3O_3$ Calculated: C: 69.4, H: 4.38, N: 12.17; Found: C: 68.56, H: 4.28, N: 12.15." Molar conductance (DMSO): 4.7 $\Omega^{-1}.mol^{-1}.cm^2$.

2.3. Synthesis of the Schiff Base-Transition Metal Structures

All structures were manufactured in a similar manner. To a stirred solution of the synthesized ligand of (0.340 g, 1mmol) in hot absolute ethanol (20 mL), the adequate metal salts and $FeCl_3.6H_2O$ in hot absolute ethanol (15mL), were added separately. The solutions were refluxed for 3 h for complete precipitation. Then, the products were eroded with absolute ethanol numerously and desiccated by vacuum.

2.4.[NiLCl(H2O)$_3$]

Yield: 68.4 %. Decomposition Point: "250 °C. IR, ν(cm^{-1}): 1669 (C=N), 1530 (C=N), 1240 (C-O), 510 (M-O), 450 (M-N). UV-Vis (DMSO), λ_{max} (nm): 268 ($\pi \rightarrow \pi^*$), 319 ($n \rightarrow \pi^*$), 490.0 ($^3A_{2g}(F) \rightarrow {}^3T_{1g}$ (P)). Elemental analysis (%): computed for $C_{20}H_{20}N_3O_6NiCl$: C: 50.62, H: 3.82, N: 8.73, Cl: 7.47, M: 12.37; Found: C: 50.54, H: 3.78, N: 8.69, Cl: 7.43, M: 12.35. Molar conductance (DMSO): 7.5 $\Omega^{-1}.mol^{-1}.cm^2$. μ_{eff} (BM): 3.15".

2.5.[CuLCl(H2O)$_3$]

Yield: 79.8 %. Decomposition Point: ">300 °C. IR, ν(cm^{-1}): 1669 (C=N), 1530 (C=N), 1253 (C-O), 517 (M-O), 461(M-N). UV-Vis (DMSO), λ_{max} (nm): 249 ($\pi \rightarrow \pi^*$), 330 ($n \rightarrow \pi^*$), 450.0 ($^2B_1 \rightarrow {}^2E$), 495.0 ($^2B_1 \rightarrow {}^2B_2$). Elemental analysis (%): computed for $C_{20}H_{20}N_3O_6CuCl$, C: 50.11, H: 3.78, N: 8.77, Cl: 7.40, M: 13.26; Found: C: 50.04, H: 3.71, N: 8.75, Cl: 7.39, M, 13.23. Molar conductance (DMSO): 11.8 $\Omega^{-1}.mol^{-1}.cm^2$. μ_{eff} (BM): 1.70".

2.6.[ZnLCl(H2O)$_3$]

Yield: 81.2%. Decomposition Point: "280 °C. ^{1}H NMR (850.000 MHz, DMSO-d_6): δ (ppm): 9.00 (s, 1H, HC=N), 8.90 (s, 1H, HC=N), 8.23-6.49 (m, 12H, Ar-H). IR, ν(cm^{-1}): 1667 (C=N), 1530 (C=N), 1238(C-O), 523 (M-O), 453(M-N). UV-Vis (DMSO), λ_{max} (nm): 244 ($\pi \rightarrow \pi^*$), 327 ($n \rightarrow \pi^*$). Elemental analysis (%): computed for $C_{20}H_{20}N_3O_6ZnCl$, C: 49.92, H: 3.77, N: 8.73, Cl: 7.37, M: 13.59; Found: C: 49.88, H: 3.75, N: 8.69, Cl: 7.35, M: 13.52. Molar conductance (DMSO): 13.4 $\Omega^{-1}.mol^{-1}.cm^2$. μ_{eff} (BM): Diamagnetic".

2.7.[CoLCl(H2O)$_3$]

Yield: 89.8%. Decomposition Point: "290 °C. IR, ν(cm^{-1}): 1670 (C=N), 1530 (C=N), 1255 (C-O), 514 (M-O), 459(M-N). UV-Vis (DMSO), λ_{max} (nm): 238 ($\pi \rightarrow \pi^*$), 329 ($n \rightarrow \pi^*$), 370 ($^4T_{1g}(F) \rightarrow {}^4T_{1g}$ (P)), 518 ($^4T_{1g}(F) \rightarrow {}^4A_{2g}$). Elemental analysis (%): computed for $C_{20}H_{20}N_3O_6NiCl$,: C: 50.60, H: 3.82, N: 8.85, Cl: 7.47, M: 12.48; Found: C: 50.55, H: 3.79, N: 8.82, Cl: 7.46, M: 12.46. Molar conductance (DMSO): 9.1 $\Omega^{-1}.mol^{-1}.cm^2$. μ_{eff} (BM): 4.19".

2.8.[FeLCl$_2$(H2O)$_2$] Structure

Yield: 75.6%. "Decomposition Point: >300 °C. IR, ν(cm^{-1}): 1651 (C=N), 1530 (C=N), 1239 (C-O), 520 (M-O), 446 (M-N). UV-Vis (DMSO), λ_{max} (nm): 258 ($\pi \rightarrow \pi^*$), 325 ($n \rightarrow \pi^*$), 381 ($^4T_{2g}(G) \rightarrow {}^6A_{1g}$), 462 ($^4T_{2g}(G) \rightarrow {}^6A_{1g}$), 492.0 ($^4T_{2g}(P) \rightarrow {}^6A_{1g}$). Elemental analysis (%): computed for $C_{20}H_{18}N_3O_5FeCl_2$, C: 49.11, H: 3.30, N: 8.59, Cl: 14.50, M: 11.42; Found: C: 49.04, H: 3.27, N: 8.56, Cl: 14.47, M: 11.39. Molar conductance (DMSO): 23.1 $\Omega^{-1}.mol^{-1}.cm^2$. μ_{eff} (BM): 5.94".

2.9. Antimicrobial Activity

The prepared Schiff base ligand and its Fe(III), Co(II), Ni(II), Cu(II), and Zn(II) structures were diluted with DMSO to produce 0.3185 mol/L of the SB ligand and 0.2317 mol/L for all structures and were experimeted for their activities against *Salmonella typhi* and *C. albicans* using the hole plate diffusion method [24,25]. Various amounts of each compound (30, 20, and 10 µL) have been introduced into each hole using a sterile micropipette tip. Gentamicin (10 µg/mL) was utilized as an affirmative control for the antibacterial assay and clotrimazole (10 µg/mL) for the antifungal assay.

2.10. Anticancer Activity

Briefly, 80% of the confluent proliferating cells were trypsinized, sowed into a 96-well plate, and refined for 24 h. Subsequently, the plate was washed with glacial acetic acid (1% v/v), for removing any staining. Then, the IC_{50} values (drug dose that eradicates survival to 50%) were determined [27].

3. Results and discussion

3.1. Chemistry

The 2-[(E)-[4-[(E)-(4-nitrophenyl)methyleneamino]phenyl]iminomethyl]phenol was prepared by refluxing 2-hydroxybenzaldehyde, 4-nitrobenzaldehyde and *p*-phenylenediamine utilizing a method previously reported by Sevens et al. [10]. The synthesized SB compound was dissolved fairly in organic solvents including MeOH, EtOH, DMF, and DMSO, whereas the metal compounds were found to be inexplicable in water and moderately soluble. The data obtained from instrumental analyses confirmed the desired compounds, as shown in Schemes 1 and 2.

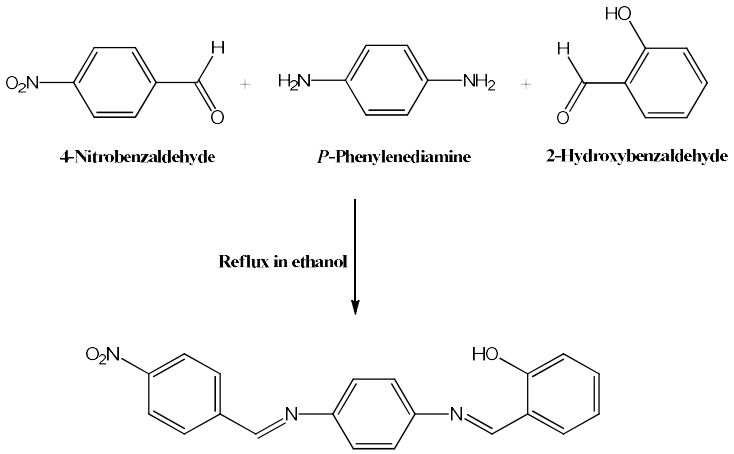

Scheme 1. Preparation scheme for the Schiff base ($C_{20}H_{15}O_3N_3$).

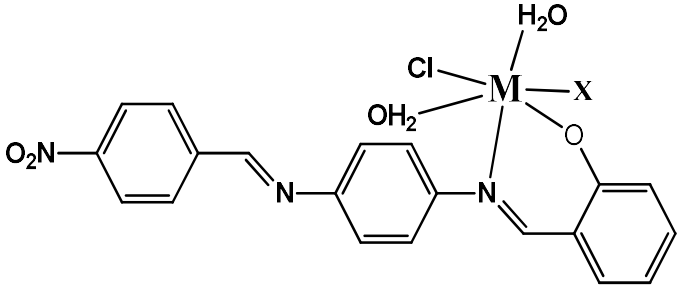

When X=H_2O, M=Ni(II), Cu(II), Zn(II), and Co(II), and when X=Cl, M=Fe(III)

Scheme 2. Proposed structures of Schiff base-transition metal structures.

3.2. ^{1}H NMR Spectroscopy:

^{1}H NMR spectroscopy of the prepared Schiff base ligand ($C_{20}H_{15}O_3N_3$) was performed using DMSO-d_6 as the solvent. ^{1}HNMR spectrum of the Schiff base is exhibited in Figure 1. The observed chemical shifts confirmed the expected structure of the Schiff base ligand. All the aromatic protons of the free ligand occurred in the expected aromatic region (6.9–8.3 ppm) as structure multiplets [28]. The two strong singlets at 8.9 and 9.0 ppm are attributed to the HC=N protons [29]. The singlet at 13.0 ppm (downfield region) is attributed to the phenolic proton [28,29]. The ^{1}H NMR spectrum of Zn(II) structure, presented in Figure S2, revealed the absence of the singlet of phenolic proton, confirming the engagement of the oxygen in structureation to Zn(II) metal [4]. The chemical shift values of other hydrogens (δ_H) are close to the appropriate (δ_H)values identified in the ^{1}H NMR spectrum of the free ligand.

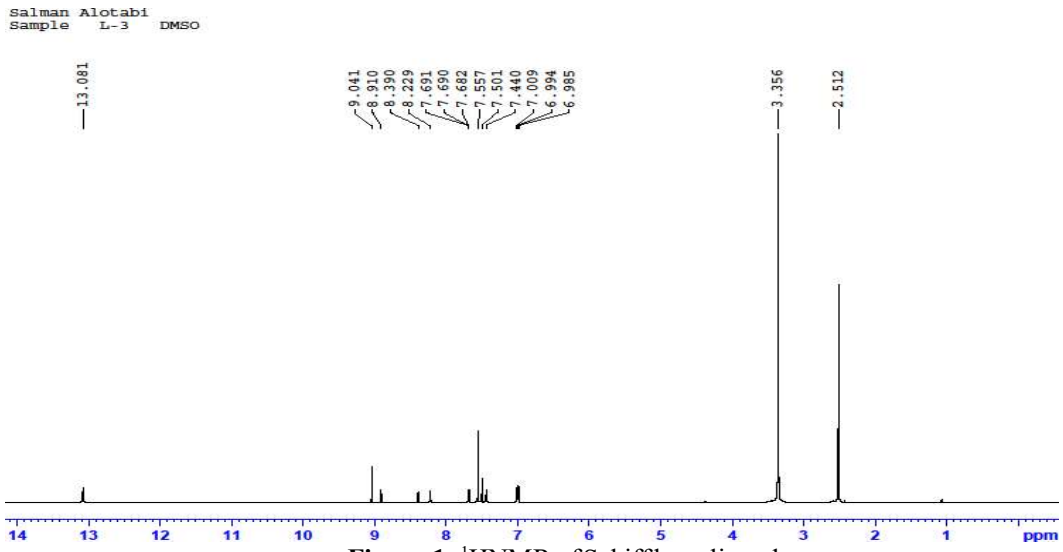

Figure 1. [1]HNMR of Schiff base ligand

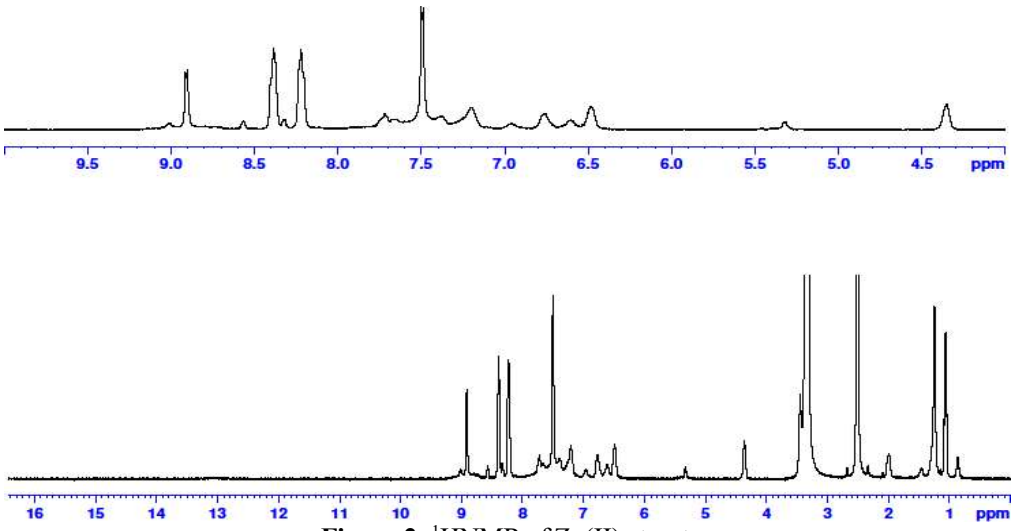

Figure 2. [1]HNMR of Zn(II) structure

3.3. [13]C NMR Spectroscopy:

[13]C NMR spectrum of Schiff base is presented in Figure S3. It exhibited signals at 163.67, 160.77, and 159.14 ppm. These signals are attributed to the phenolic, azomethine, and azomethine carbons, respectively [28]. Signals that appeared in the range 117.09–149.69 ppm are ascribed to the aromatic carbons [29].

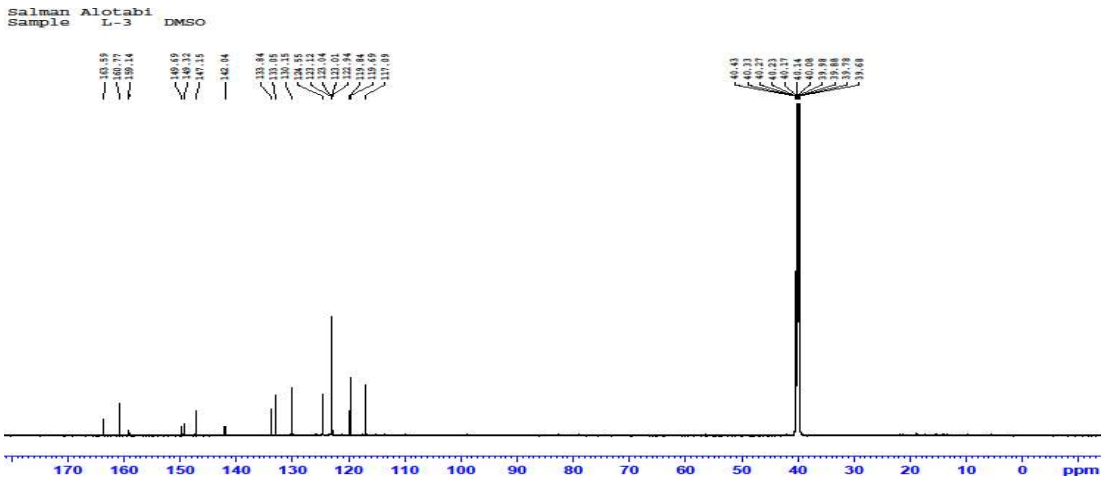

Figure 3. ^{13}CNMR of Schiff base ligand

3.4. FT-IR and Far Infrared Spectroscopies

The high-intensity bands of the Schiff base ligand at 1662 and 1530 cm^{-1} can be characterized to the widening modes of the azomethine [28,29] group. The broadband of the Schiff base ligand at 3100 cm^{-1} is ascribed to the phenolic group [29]. Shifting of the band position belongs to the C=N band modes at 1662 cm^{1} in the IR ranges of the organized transition metal structures confirms that azomethine group is structureed with the transition metals [28]. The new broad bands in the structures at 3600–3300 cm^{-1} could be allocated to the symmetric and asymmetric stretching methods of the coordinated water molecules [23]. Moreover, the band belongs to the widening mode of C-O bonds found in the free Schiff base at 1245 cm^{-1} is also shifted in the IR ranges of the metal structures settling the deprotonation and development of phenolate type (N,N,O) coordinated Schiff base-transition metal structures [29]. The bands of M-O were experiential in the area of 510–523 cm^{-1} and the bands ascribed to M-N bands occurred in the area of 446–461 cm^{-1} [4].

Table 1. Characteristic IR absorption bands (cm^{-1}) of the prepared Schiff base ligand and its metal (II) and Metal (III) structures

Compound	*ν*(OH)	*ν*(C=N)	*ν*(C-O)	*ν*(M-O)	*ν*(M-N
L = $C_{20}H_{15}O_3N_3$	3100	1662–1530	1245	-	-
[NiLCl(H_2O)3]	-	1659–1530	1240	510	450
[CuLCl(H_2O)$_3$]	-	1669–1530	1253	517	461
[ZnLCl(H_2O)3]	-	1667–1530	1238	523	453
[CoLCl(H_2O)3]	-	1670–1530	1255	514	459
[FeLCl2(H_2O)$_2$]	-	1651–1530	1239	520	446

3.5. CHN Analyses

All the data obtained from the CHN elemental analyzer were in effective pattern with the prepared structures and the calculated values of the C, H, and N content. The found values agreed with the anticipated values (Table 2).

Table 2. Physical data and analytical properties of the Schiff base and its transition metal structures

Compound	D.P. (°C)	M	C	H	N	Cl
		Calculated (Found) (%)				
L = $C_{20}H_{15}O_3N_3$	160	-	69.56 (69.54)	4.38 (4.33)	12.17(12.1)	-
[NiLCl(H_2O)3]	250	12.37 (12.35)	50.62 (50.54)	3.82 (3.78)	8.73 (8.69)	7.47 (7.43)
[CuLCl(H_2O)$_3$]	>300	13.26 (13.23)	50.11 (50.04)	3.78 (3.71)	8.77 (8.75)	7.40 (7.39)
[ZnLCl(H_2O)3]	280	13.59 (13.52)	49.92 (49.88)	3.77 (3.75)	8.73 (8.69)	7.37 (7.35)
[CoLCl(H_2O)3]	290	12.48 (12.46)	50.60 (50.55)	3.82 (3.79)	8.85 (8.82)	7.47 (7.46)
[FeLCl2(H_2O)$_2$]	>300	11.42(11.39)	49.11 (49.04)	3.30 (3.27)	8.59 (8.56)	14.50 (14.47)

3.6. Electronic (UV-Visible) Ranges

The UV-Visible (UV-Vis) spectrum of each compound was documented in DMSO (1×10^{-4} M, Table 3). The spectrum of 2-[(E)-[4-[(E)-(4-nitrophenyl)methyleneamino]phenyl]iminomethyl]phenol exhibits bands at 250 and 325 nm, which are ascribed to the $\pi \rightarrow \pi^*$ changes of the C=C aromatic rings and $n \rightarrow \pi^*$ changes of C=N azomethine groups, respectively [30,31]. These bands are shifted in the ranges of metal structures, which can be attributed to the metal-ligand coordination [30]. The electronic ranges of the Ni(II), Cu(II), Co(II) and Fe(III) structures exhibits d-d transitions at 490 nm (spin-allowed $^3A_{2g}(F) \rightarrow {}^3T_{1g}(P)$), at 450 and 495 nm ($^2B_1 \rightarrow {}^2E$ and $^2B_1 \rightarrow {}^2B_2$, respectively), at 370 and 518 nm and at 381, 462, and 492 nm indicating octahedral arrangements in all four structures [23, 30–33]. The Zn(II) structure has completely filled d orbitals and does not shows any d-d transition.

Table 3. Electronic UV-Vis rangesl assignments.

Compound	π-π* (nm)	*n*-π* (nm)	*d-d* (nm)
L = $C_{20}H_{15}O_3N_3$	250	325	-
[NiLCl(H_2O)3]	268	319	490
[CuLCl(H_2O)$_3$]	249	330	450, 495
[ZnLCl(H_2O)3]	244	327	-
[CoLCl(H_2O)3]	238	329	370, 518
[$FeLCl_2$(H_2O)$_2$]	258	325	381, 462, 492

3.8. Molar Conductivity

The molar conductivities (10^{-3} M) of the prepared structures dissolved in DMSO were determined at room temperature (Table 4) This is further supported by adding $AgNO_3$ solution to the structures and no white precipitate has formed, confirming that all chlorine ions are involved in coordinating with the metals and not located outside the coordination sphere [30,32].

3.9. Magnetic Moment

The room temperature magnetic moments are listed in Table 4. The magnetic moment of the Ni(II) structure was 3.15 BM [33], whereas, for Cu(II) structure, it was 1.70 BM, indicating one unpaired electron in the outer valence shell [34] and an octahedral geometry. The Co(II) structure exhibited 4.19 BM, owing to the occurrence of three ungrouped electrons in the outer valence shell [34], whereas Fe(III) structure demonstrated a magnetic moment of 5.94 BM, suggesting an octahedral geometry [35].-The Zn(II) structure is diamagnetic owing to its d^{10} formation [11].

Table 4. Molar conductivities and magnetic moments for the prepared Schiff base and its transition metal structures

Compound	Molar Conductivity $\Omega^{-1}.mol^{-1}.cm^2$	Magnetic Moment B.M
L = C20H15O3N3	4.7	-
[NiLCl(H2O)3]	7.5	3.15
[CuLCl(H2O)3]	11.8	1.70
[ZnLCl(H2O)3]	13.4	Diamagnetic
[CoLCl(H2O)3]	9.1	4.19
[FeLCl2(H2O)2]	23.1	5.94

3.10. Thermogravimetric Analyses

Figures 5–9 show the TGA curves of all the prepared transition metal structures. They exhibited three steps of thermal decomposition. The first step was in the 150–245 °C range, where the Ni(II), Cu(II), Zn(II), and Co(II) structures lost 10% of three coordinated water molecules, and Fe(III) structure lost 7% of two synchronized water molecules [35]. The calculated mass losses agreed well with the experimental ones (Table S2). The second decomposition step occurred over 250 °C covers with each other and belong to the loss of chloride content (as HCl), 7% for the Ni(II), Cu(II), Zn(II) and Co(II), and 14% for Fe(III). The third step is the degradation of Schiff base ligand [35,36]. The overall weight loss (70.12–75.08%) agrees well with the development of the appropriate metal oxides [37,38].

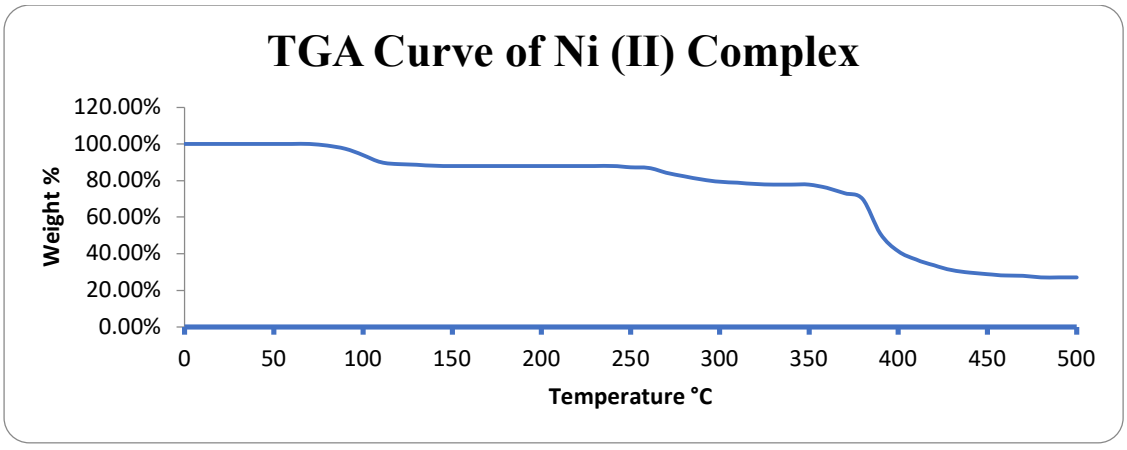

Figure 5. The TGA curve of Ni(II) structure

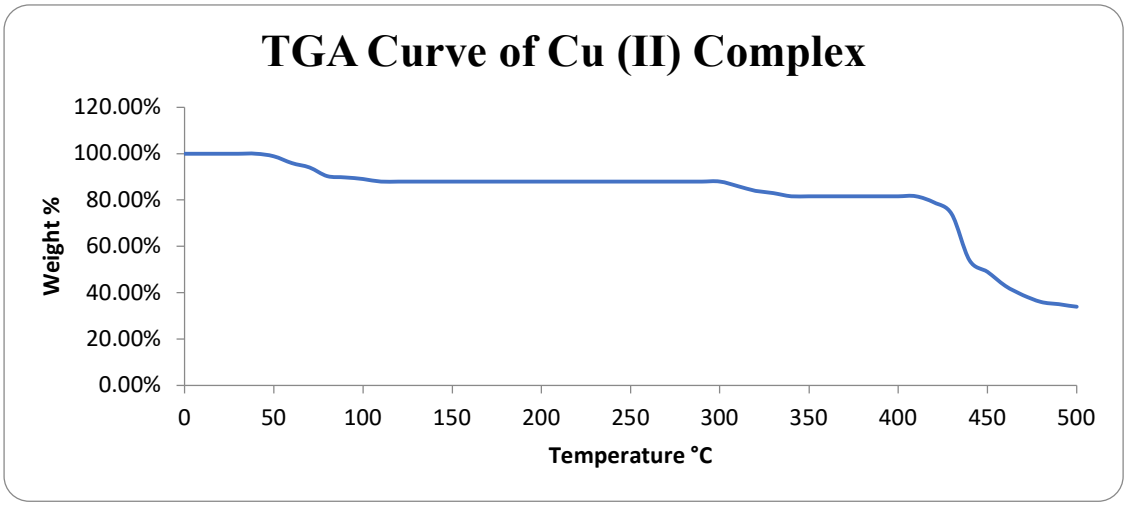

Figure 6. The TGA curve of Cu(II) structure

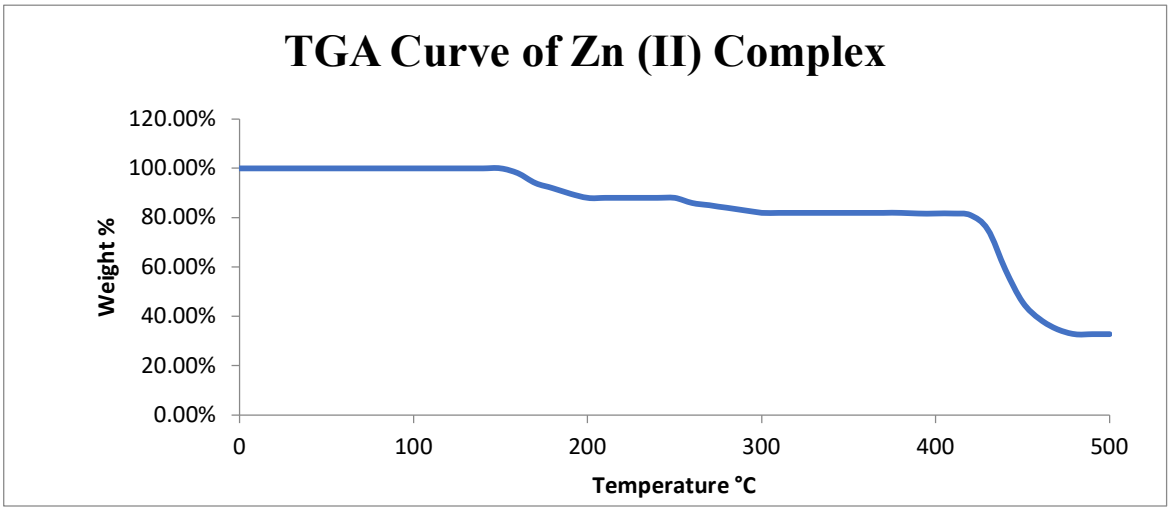

Figure 7. The TGA curve of Zn(II) structure

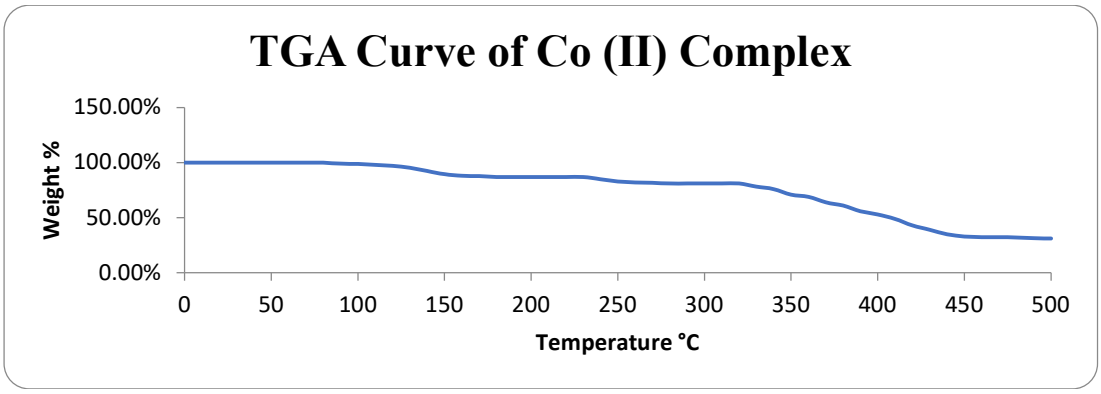

Figure 8. The TGA curve of Co(II) structure.

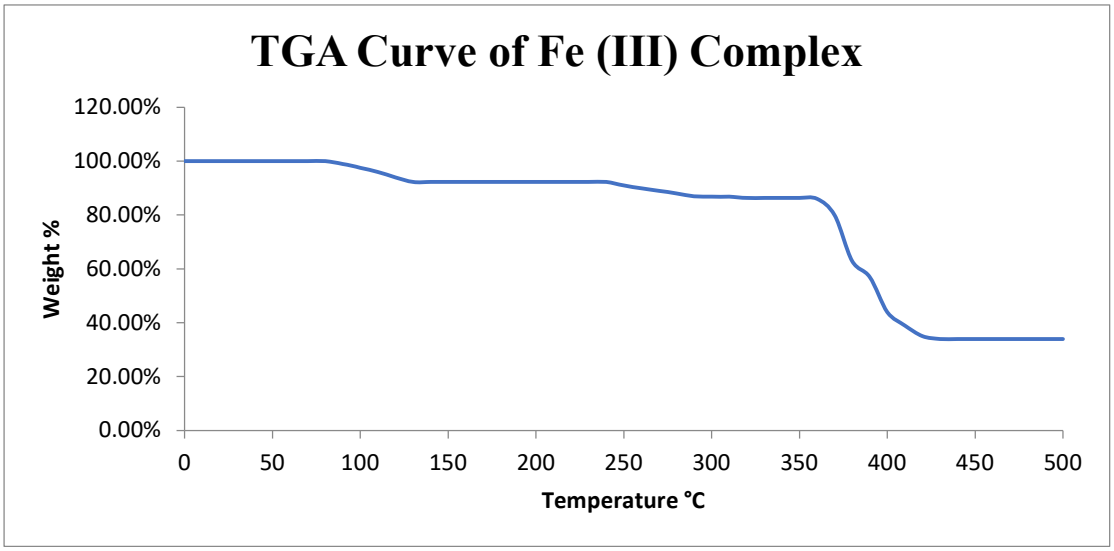

Figure 9. The TGA curve of Fe(III) structure

3.11. X-Ray Diffraction Analysis

X-ray diffractions patterns (XRD) are presented in Figure 7. They were collected at room temperature. The crystal structure data of the synthesized materials are presented in Table 5. The Fe(III), Co(II), Ni(II), Cu(II), and Zn(II) structures possessed crystal sizes in the range 17.10–35.40 nm, indicating that they are on a nanometre scale. This is also supported by peak widening in the XRD trends, which indicates that the particles were on a nanometre scale. These parameters can be acquired free of charge from http://www.crystallography.net/cod/.

Table 5. XRD analysis data for all structures.

Structure	a (Å)	b (Å)	c (Å)	α (°)	β (°)	γ (°)	Cell Volume (Å)	Crystal Size (nm)	Crystal Type	Space Group
Ni(II)	8.7	6.4	7.7	90.0	90.0	90.0	2671.482	17.10	orthorhombic	*P mmm*
Cu(II)	6.2	19.9	14.8	90.0	90.0	90.0	1663.36	32.30	orthorhombic	*P bmn*
Zn(II)	5.6	5.6	8.0	90.0	90.0	120.0	2610.47	19.60	hexagonal	*P-6*
Co(II)	8.5	11.7	13.0	90.0	92.0	90.0	1292.06	25.90	monoclinic	$P2_1/c$
Fe(III)	11.4	11.4	11.4	90.0	90.0	90.0	1481.54	35.40	cubic	*Pa-3*

4. Biological Activity

4.1. Antibacterial Activity

In vitro antibacterial activities of the Schiff base ligand and its structures against *Salmonella typhi* are listed in Table 6. The findings indicated that the ligand and its Zn(II), Co(II), and Fe(III) structures did not show antibacterial activity. In contrast, the Ni(II) structure demonstrated intermediate activity across all sample volumes and the Cu(II) structure portrayed intermediate activity at the sample volumes of 20 µL and 10 µL and high activity at 30 µL (Figure S8). Notably, Ni(II) and Cu(II) structures demonstrated higher

antibacterial activities than that of the free Schiff base ligand. The Ni(II) and Cu(II) structures have manifested greater results against *Salmonella typhi* than the results obtained by Alorini et al. [30].

Table 6. Antibacterial activities of the Schiff base ligand and its metal structures.

Compound	Volumes			
	30 µL	20 µL	10 µL	mycin (10 µg/mL) Positive Control
L = $C_{20}H_{15}O_3N_3$	0	0	0	2
[NiLCl(H2O)3]	9	7	6	
[CuLCl(H2O)$_3$]	12	10	6	
[ZnLCl(H2O)3]	0	0	0	
[CoLCl(H2O)3]	0	0	0	
[FeLCl2(H2O)$_2$]	0	0	0	

4.2. Antifungal Activity

The antifungal occurrences of the Schiff base and its metal structures took in three different sample volumes were assessed against *Candida albicans* growth Table 7. Figure S displays active compounds against *C. albicans*. The Ni(II) structure portrayed a high antifungal activity at 30 µL and intermediate activities at 20 µL and 10 µL. The Cu(II) structure demonstrated the highest antifungal activities at 30 µL and 20 µL and intermediate activity at 10 µL. The Schiff base ligand and Co(II) structure showed intermediate antifungal activities at 30 µL and 20 µL and weak activity at 10 µL. However, Zn(II) and Fe(III) structures did not show antifungal activities against *C. albicans* growth. Higher antifungal activities for Ni(II) and Cu(II) structures and equal antifungal activity for Co(II) structure were observed in comparison with the study performed by Gomathi et al. [38].

Table 7. Antifungal activities of the Schiff base ligand and its metal structures.

Compound	Volumes			
	30 µL	20 µL	10 µL	nazole (10 µg/mL Positive Control)
L$C_{20}H_{15}O_3N_3$	6	5	3	2
[NiLCl(H2O)3]	12	10	6	
[CuLCl(H2O)$_3$]	13	11	6	
[ZnLCl(H2O)3]	0	0	0	
[CoLCl(H2O)3]	9	7	3	
[FeLCl2(H2O)$_2$]	0	0	0	

4.3. Anticancer Activities

The anticancer activities of the free ligand and its Ni(II), Cu(II), Zn(II), Co(II), and Fe(III) metal structures were evaluated against PC-3, SKOV3, and HeLa cell lines. Final concentrations of the Schiff base ligand used to analyze the anticancer activities were 0.000029, 0.00029, 0.0029, 0.029, 0.29, and 2.9 mM; of the Ni(II), Cu(II), Zn(II), and Co(II) structures were 0.000021, 0.00021, 0.0021, 0.021, 0.21, and 2.1 mM; and of the Fe(III) structure were 0.000020, 0.00020, 0.0020, 0.020, 0.20, and 2.0 mM. Table 8 discloses the IC_{50} values for the free ligand and its structures. By comparing the obtained IC_{50} values with those in a previous report by Aroua et al., we deduced that the synthesized compounds in our study demonstrated considerable anticancer activities alongside the chosen human cell lines [23]. However, the Fe(III) structure showed weak anticancer activity against PC-3 cancer cells, and the Ni(II) structure demonstrated a moderate effect on SKOV3 cancer cells. Notably, the Cu(II) structure exhibited the highest anticancer activity (IC_{50} = 0.0002 and 0.0001 mM) against SKOV3 and HeLa cells.

Table 8. IC_{50} values (mM) of the prepared compounds against PC-3, SKOV3, and Hela cancer cells**.**

Compound	PC-3	SKOV3	HeLa
Doxorubicin	$4.80\times10^{-3}\pm4.00\times10^{-5}$	$4.00\times10^{-3}\pm4.00\times10^{-4}$	$3.50\times10^{-3}\pm7.00\times10^{-5}$
$L = C_{20}H_{15}O_3N_3$	$1.53\times10^{-2}\pm1.90\times10^{-3}$	$1.30\times10^{-2}\pm2.00\times10^{-3}$	$1.53\times10^{-2}\pm2.60\times10^{-3}$
[NiLCl(H2O)3]	ł$1\times10^{-2}\pm3.00\times10^{-3}$	$3.03\times10^{-2}\pm2.50\times10^{-3}$	$3.20\times10^{-3}\pm6.00\times10^{-4}$
$[CuLCl(H2O)_3]$	$4.40\times10^{-3}\pm5.00\times10^{-4}$	$2.00\times10^{-4}\pm2.00\times10^{-5}$	$1.00\times10^{-4}\pm2.00\times10^{-4}$
[ZnLCl(H2O)3]	$5.60\times10^{-3}\pm8.00\times10^{-4}$	$1.50\times10^{-3}\pm2.00\times10^{-4}$	$7.30\times10^{-3}\pm1.00\times10^{-3}$
[CoLCl(H2O)3]	$1.87\times10^{-2}\pm1.50\times10^{-3}$	$6.00\times10^{-4}\pm2.00\times10^{-4}$	$1.30\times10^{-3}\pm4.00\times10^{-4}$
$[FeLCl2(H2O)_2]$	$6.42\times10^{-2}\pm2.20\times10^{-3}$	$2.70\times10^{-3}\pm2.00\times10^{-4}$	$1.27\times10^{-2}\pm2.20\times10^{-3}$

Conclusions

In this study, facile synthetic methods for a Schiff base and its change metal structures (Fe(III), Ni(II) Cu(II), Co(II), Zn(II)) were demonstrated. The Schiff base was prepared from 4-nitrobenzaldehyde, 2-hydroxybenzaldehyde, and *p*-phenylenediamine. Characterization of the as-synthesized materials via FT-IR, and UV-Vis spectroscopy, CHN elemental and thermogravimetric analyses, X-Ray Diffraction Analysis, molar conductivity, and magnetic vulnerability capacities revealed that all the structures own an octahedral geometry. The assessment of in vitro antibacterial and antifungal happenings of the manufactured Schiff base and its polymeric transition metal structures showed that only Ni(II) and Cu(II) structures portrayed the highest activities in contradiction of *S. typhi* and *C. albicans*. All structures, except the Fe(III) structure against PC-3 cells, demonstrated considerable anticancer activities in contradiction of PC-3, SKOV3, and HeLa cell lines.

References:

[1] T.T. Tidwell, Hugo (Ugo) Schiff, Schiff bases, and a century of β-lactam synthesis. Angew. Chem. Int. Ed. vol. 47, no. 6, pp. 1016–1020, 2008. https://doi.org/10.1002/anie.200702965

[2] H. Schiff, Eine neue Reihe organischer Basen. Annalen Der Chemie und Pharmacie. Vol. 131, no. 1, pp. 118–119, 1864. doi:10.1002/jlac.18641310113

[3] Y. Hijji, R. Rajan, H. Ben Yahia, S. Mansour, A. Zarrouk, I. Warad, One-Pot microwave-assisted synthesis of water-soluble pyran-2,4,5-triol glucose amine Schiff base derivative: XRD/HSA interactions, crystal structure, rangesl, thermal and a DFT/TD-DFT. *Crystals*. vol. *11*, no. 2, pp. 117, 2021. https://doi.org/10.3390/cryst11020117

[4] H.B. Howsaui, A.A. Sharfalddin, M.H. Abdellattif, A.S. Basaleh, M.A. Hussien, Synthesis, spectroscopic characterization and biological studies of Mn(II), Cu(II), Ni(II), Co(II) and Zn(II) structures with new Schiff base of 2-((Pyrazine-2-ylimino)methyl)phenol. *Appl. Sci.* vol. 11, no. 19 pp. 9067, 2021. https://doi.org/10.3390/app11199067

[5] A. Reiss, N. Cioateră, A. Dobrițescu, M. Rotaru, A.C. Carabet, F. Parisi, A. Gănescu, I. Dăbuleanu, C.I. Spînu, P. Rotaru, Bioactive Co(II), Ni(II), and Cu(II) structures containing a tridentate sulfathiazole-based (ONN) Schiff base. *Molecules.* vol. *26*, no. 19, pp. 3062, 2021. https://doi.org/10.3390/molecules26103062

[6] L.H. Abdel-Rahman, M.A. Adam, A.M. Abu-Dief, H.E-s. Ahmed, A. Nafady, Non-Linear optical property and biological assays of therapeutic potentials under in vitro conditions of Pd(II), Ag(I) and Cu(II) structures of 5-diethyl amino-2-({2-[(2-hydroxy-Benzylidene)-amino]-phenylimino}-methyl)-phenol. *Molecules.* vol. *25, no. 21*, pp. 5089, 2020. https://doi.org/10.3390/molecules25215089

[7] S.N.A. Bukhari, M.Y. Zakaria, M.U. Munir, N. Ahmad, M.A. Elsherif, R.E. Badr, A.K. Hassan, A.H.A. Almaaty, I. Zaki, Design, synthesis, in vitro biological activity evaluation and stabilized nanostructured lipid carrier formulation of newly synthesized Schiff bases-based TMP moieties. *Pharmaceuticals.* vol. *15*, no. 6, pp. 679, 2022. https://doi.org/10.3390/ph15060679

[8] A. Alam, M. Ali, N.U. Rehman, S. Ullah, S.A. Halim, A. Latif, Zainab, A. Khan, O. Ullah, S. Ahmad, A. Al-Harrasi, M. Ahmad, Bio-Oriented synthesis of novel (S)-Flurbiprofen Clubbed Hydrazone Schiff's bases for diabetic management: In vitro and in Silico Studies. *Pharmaceuticals*. vol. *15*, no. 6, pp. 672, 2022. https://doi.org/10.3390/ph15060672

[9] H.F.G Barbosa, E.T.G. Cavalheiro, The influence of reaction parameters on structureation of Zn(II) structures with biopolymeric Schiff bases prepared from chitosan and salicylaldehyde. Int. J. Biol. Macromol. Vol. 121, pp. 1179–1185, 2019. https://doi.org/10.1016/j.ijbiomac.2018.10.113

[10] Sevens et al. Bulletin des Societes Chimiques Belges, **1948**, *57*, 32.

[11] E. Canpolat, M. Kaya, Studies on mononuclear chelates derived from substituted Schiff bases ligands (Part 3). Synthesis and characterization of a new 5-nitrosalicylidene-p-aminoacetophenoneoxime and its structures with Co(II), Ni(II), Cu(II), and Zn(II). J. Coord. Chem. vol. 58, no, 12, pp. 1063–1069, 2007. https://doi.org/10.1080/00958970500122565

[12] T.M.A. Al-Shboul, M. El-khateeb, A.H. Obeidat, T.S. Ababneh, S.S. Al-Tarawneh, M.S. Al Zoubi, W. Alshaer, A. Abu Seni, T. Qasem, H. Moriyama, Y. Yoshida, H. Kitagawa, T.M.A. Jazzazi, Synthesis, characterization, computational and biological activity of some Schiff bases and their Fe, Cu and Zn structures. *Inorganics*. vol. *10*, no. 8, pp. 112, 2022. https://doi.org/10.3390/inorganics10080112
[13] R.A. Ambhure, S.R. Mirgane, D.U. Thombal, S.U. Shisodia, S.S. Pandule, L. Kótai, R.P. Pawar, Synthesis and antimicrobial activity of imines and their metal structures, Eur. Chem. Bull. vol. 5, no. 10, pp. 428-430, 2016. DOI: 10.17628/ECB.2016.5.428
[14] J. Magyari, B.B. Holló, L.S. Vojinović-Ješić, M.M. Radanović, S. Armaković, S.J. Armaković, J. Molnár, A. Kincses, M. GAjdács, G. Spengler, K.M. Szecsenyi, Interactions of Schiff base compounds and their coordination structures with the drug cisplatin. New J. Chem. vol. 42, pp. 5834-5843, 2018. DOI: 10.1039/C8NJ00357B
[15] A.S. Kauthale, S. Tekale, A. Rode, R. Patil, J. Sangshetti, L. Kótai, R.P. Pawar, Eaton's reagent catalyzed synthesis, in vitro □-amylase inhibitory activity and molecular docking study of some Schiff bases as diabetic inhibitors, Eur. Chem. Bull. vol. 8, pp. 356-362, 2019. http://dx.doi.org/10.17628/ecb.2019.8.356-362
[16] S.P. Bhale, A.R. Yadav, P.G. Pathare, S.U. Tekale, F.P. Franguelli, L. Kótai, R.B. Pawar, Synthesis, characterization and antimicrobial activity of transition metal structures of 4-[(2-hydroxy-4-methoxyphenyl)methyleneamino]-2,4-dihydro-3H-1,2,4-triazole-3-thione, Eur. Chem. Bull. vol. 9, pp. 430-435, 2020. http://dx.doi.org/10.17628/ecb.2020.9.430-435
[17] G. Backes, D. Neumann, B. Jursic, Synthesis and antifungal activity of substituted salicylaldehyde hydrazones, hydrazides and sulfohydrazides. Bioorg. Med. Chem. 2014, vol. 22, pp. 4629–4636, 2014. https://doi.org/10.1016/j.bmc.2014.07.022
[18] P. Jayaseelan, S. Prasad, S. Vedanayaki, R. Rajavel, Synthesis, rangesl characterization, electrochemical and anti-microbial activities of new binuclear Schiff base metal structures derived from 3,3' diaminobenzedine. *Euro. J. Chem.* Vol. 4, 480–484, 2011. DOI:10.5155/eurjchem.2.4.480-484.353
[19] L.A. Saghatforoush, A. Aminkhani, F. Chalabian, Iron(III) Schiff base structures with asymmetric tetradentate ligands: synthesis, spectroscopy, and antimicrobial properties. Transit. Met. Chem. vol. 34, pp. 899–904, 2009. https://doi.org/10.1007/s11243-009-9279-8
[20] M.S. Refat, L.M. El-Deen, Z.M. Anwer, S. El-Ghol, Spectroscopic studies and biological evaluation of some transition metal structures of Schiff-base ligands derived from 5-arylazo-salicylaldehyde and thiosemicarbazide. J. Coord. Chem. vol. 62, pp. 1709–1718, 2009. https://doi.org/10.1080/00958970802684205
[21] C.D. Sheela, C. Anitha, P Tharmaraj, D. Kodimunthri, Synthesis, rangesl characterization, and antimicrobial studies of metal structures of the Schiff base derived from [4-amino-N-guanylbenzene sulfonamide] and salicylaldehyde. J. Coord. Chem. vol. 63, no. 5, pp. 884–893, 2010. https://doi.org/10.1080/00958971003660416
[22] Aragón-Muriel, A.; Liscano, Y.; Upegui, Y.; Robledo, S.M.; Ramírez-Apan, M.T.; Morales-Morales, D.; Oñate-Garzón, J.; Polo-Cerón, D. In vitro evaluation of the potential pharmacological activity and molecular targets of new benzimidazole-based Schiff base metal structures. *Antibiotics*. Vol. *10*, no. 6, pp. 728, 2021. https://doi.org/10.3390/antibiotics10060728
[23] L.M. Aroua, A,N. Al-Hakimi, M.A.M. Abdughani, S.K. Alhag, Cytotoxic urea Schiff base structures for multidrug discovery as anticancer activity and low in vivo oral assessing toxicity. Arab J. Chem. vol. 15, pp. 103986, 2022. https://doi.org/10.1016/j.arabc.2022.103986
[24] J. Vanco, J. Marek, Z. Travnicek, E. Racanska, J. Muselik, O.G. Svajlenova, Synthesis, structural characterization, antiradical and antidiabetic activities of copper(II) and zinc(II) Schiff base structures derived from salicylaldehyde and β-alanine. J. Inorg. Biochem. Vol. 102, no. 4 pp. 595–605, 2008. https://doi.org/10.1016/j.jinorgbio.2007.10.003
[25] M.L. Magwa, M. Gundidza, N. Gweru, G. Humphrey, Chemical composition and biological activities of essential oil from the leaves of *Sesuvium portulacastrum.* J. Ethnopharmacol. Vol. 103, no. 1, pp. 85–89, 2006. https://doi.org/10.1016/j.jep.2005.07.024
[26] C. Valgas, S.M.D. Souza, E.F. Smania, A. Smania Jr, Screening methods to determine antibacterial activity of natural products. Braz. J. Microbiol. vol. 38, pp. 369–380, 2007. https://www.scielo.br/j/bjm/a/Dh8Ry8WX4vc6QmXBddcwccQ/?format=pdf&lang=en
[27] M.M. Alam, S. Nazreen, A.S Almalki, A.A. Elhenawy, N.I. Alsenani, S.E.I. Elbehairi, A.M. Malebari, M.Y. Alfaifi, M.A. Alsharif, S.Y. Alfaifi, Naproxen based 1,3,4-oxadiazole derivatives as EGFR inhibitors: Design, synthesis, anticancer, and computational studies. Pharmaceuticals. vol. 14, no. 9, pp. 870, 2011. https://doi.org/10.3390/ph14090870
[28] D. Aggoun, M. Fernandez-Garcia, M. Lopez, B. Bouzerafa, Y. Ouennoughi, F. Setifi, A. Ourari, New nickel (II) and copper (II) bidentate Schiff base structures, derived from dihalogenated salicylaldehyde and alkylamine: Synthesis, spectroscopic, thermogravimetry, crystallographic determination and electrochemical studies. Polyhedron, vol. 187, pp. 114640, 2020. https://doi.org/10.1016/j.poly.2020.114640
[29] A.A.A. Abdel Aziz, A.N.M. Salem, M.A. Sayed, M.M. Aboaly, Synthesis, structural characterization, thermal studies, catalytic efficiency and antimicrobial activity of some M(II) structures with ONO tridentate Schiff base N-salicylidene-o-aminophenol (saphH2). J. Mol. Struct. vol. 1010, pp. 130–138, 2012. https://doi.org/10.1016/j.molstruc.2011.11.043
[30] T.A. Alorini, A.N. Al-Hakimi, S.E.S. Saeed, E.H.L. Alhamzi, A.E. Albadri, Synthesis, characterization, and anticancer activity of some metal structures with a new Schiff base ligand. Arab. J. Chem. vol. 15, pp. 103559, 2022. https://doi.org/10.1016/j.arabjc.2021.103559

[31] M. Mesbah, M. Douadi, F. Sahli, S. Issaadi, S. Boukazoula, S. Chafaa, Synthesis, characterization, spectroscopic studies and antimicrobial activity of three new Schiff bases derived from Heterocyclic moiety. J. Mol. Struct. vol. 1151, pp. 41–48, 2018. https://doi.org/10.1016/j.molstruc.2017.08.098
[32] P. Jayaseelan, S. Prasad, S. Vedanaki, R. Rajavel, Synthesis, characterization, antimicrobial, DNA binding and cleavage studies of Schiff base metal structures. Arab. J. Chem. vol. 9, pp. S668–S677, 2016. https://doi.org/10.1016/j.arabjc.2011.07.029
[33] M.S. Al-Fakeh, G.A. Allazzam, N.H. Yarkandi, Ni(II), Cu(II), Mn(II), and Fe(II) Metal Structures Containing 1,3-Bis(diphenylphosphino)propane and Pyridine Derivative: Synthesis, Characterization, and Antimicrobial Activity. Int. J. Biomater. pp. 2021, 2021. https://doi.org/10.1155/2021/4981367
[34] M.S. Alfakeh, Synthesis, thermal stability, and kinetic studies of copper (II) and cobalt (II) structures derived from 4-aminobenzohydrazide and 2-mercaptobenzothiazole. Eur. Chem. Bull. vol. 9, 403–409, 2020. https://dx.doi.org/10.17628/ecb.2020.9.403-409
[35] V. Muraskova, V. Eigner, M. Dusek, D. Sedmidubsky, Iron(III) and cobalt(III) structures with pentadentate pyridoxal Schiff base ligand–structure, rangesl, electrochemical, magnetic properties and DFT calculations. Polyhedron. vol. 197, pp. 115019, 2021. https://doi.org/10.1016/j.poly.2021.115019
[36] J. Devi, M. Yadav, Synthesis and characterization of transition metal structures of Schiff bases derived from 3-formyl chromone. Asian J. Chem. vol. 29, pp. 551–554, 2017. https://doi.org/10.14233/ajchem.2017.20236
[37] S.A. Abdel-Latif, H.B. Hassib, Y.M. Issa, Studies on some salicylaldehyde Schiff base derivatives and their structures with Cr(III), Mn(II), Fe(III), Ni(II) and Cu(II). Spectrochim. Acta A Mol. Biomol. Spectrosc. vol. 67, pp. 950–957, 2007. https://doi.org/10.1016/j.saa.2006.09.013
[38] T. Gomathi, S. Karthik, S. Vedanayaki, Synthesis, rangesl, electrochemical and biological studies on Co(II), Ni(II), Cu(II) and Zn(II) structures derived from 4-(2-Aminoethyl)benzene-1,2-diol and Terephthalaldehyde. Asian J. Chem. pp. 1373–1382, 2022. https://doi.org/10.14233/ajchem.2022.23534

تشييد والتوصيف والتقييم البيولوجي لقاعدة شيف غير المتماثلة NNO المانحة وهياكلها المعدنية الانتقالية

الملخص العربي

م تشييد ليجند قاعدة ترايدنتات شيف عبر تركيز 4-نيتروبنزالدهيد، 2-هيدروكسي بنزالدهيد، وب-فينيليندیامين وتم تجهيز وتصنيف الهياكل. تم تحديد التركيب الهيكلي لقاعدة شيف المركبة وهياكلها المعدنية باستخدام الطرق الطيفية. أكد التحليل الطيفي للرنين المغناطيسي النووي تركيب ليجند قاعدة شيف، حيث أظهر بروتونات الآزوميثين عند 8.91 و9.04 جزء في المليون في طيف 1 HNMR وكربونات الآزوميثين عند 160.77 و159.14 جزء في المليون في طيف 13 .CNMR علاوة على ذلك، ساعد التحليل الطيفي FT-IR في الكشف عن رابطة SB المحضرة وهياكلها المعدنية. على سبيل المثال، كشفت نطاقات الامتصاص عند 1662 سم-1 و1530 سم-1 في طيف FT-IR للرابطة SB عن تكوين مجموعات الآزوميثين، وتحولت هذه النطاقات إما إلى ترددات أقل أو أعلى في نطاقات الهياكل، إثبات إدارة قاعدة شيف للمعادن المختارة. في هذه الأثناء، كشف التحليل الطيفي للأشعة المرئية وفوق البنفسجية عن إثارة انتقال *π← n لمجموعة الآزوميثين عند 325 نانومتر، وبالتالي تم تحويل هذا التحول عند التركيب مع التحولات الواضحة .d-d تم استخدام الموصلية المولية وقدرات العزم المغناطيسي لدعم الأدلة على تطور الهياكل الأساسية لشيف البوليمرية. أظهرت الهياكل Ni(II) و Cu(II)أنشطة مضادة للبكتيريا والفطريات، في حين أظهرت جميع الهياكل أنشطة كبيرة مضادة للسرطان ضد الخلايا السرطانية البشرية SKOV3 وHLa